

Article

Numerical Simulation on the Effect of Fire Shutter Descending Height on Smoke Extraction Efficiency in a Large Atrium

Qiyu Liu ¹, Jianren Xiao ², Bihe Cai ³, Xiaoying Guo ², Hui Wang ⁴, Jian Chen ⁵, Meihong Zhang ⁶, Huasheng Qiu ⁷, Chunlin Zheng ⁸ and Yang Zhou ^{1,*}

¹ School of Civil Engineering, Central South University, Changsha 410075, China; liuqy99@csu.edu.cn

² Fujian Provincial Institute of Architectural Design and Research Co., Ltd., Fuzhou 350001, China; xjr@fjadi.com.cn (J.X.); gxy@fjadi.com.cn (X.G.)

³ YanGuo Technology Co., Ltd., Xiamen 361001, China; bihe.cai@csu.edu.cn

⁴ Fujian Construction Engineering Group Co., Ltd., Fuzhou 350001, China; huiwang490@csu.edu.cn

⁵ China Academy of Building Research, Beijing 100013, China; ken_chenjian@126.com

⁶ Xiamen Fire Rescue Detachment, Xiamen 361013, China; zhangmhxm@sina.com

⁷ China Construction Fourth Engineering Division Co., Ltd., Guangzhou 510665, China; hsqiu1979@csu.edu.cn

⁸ Straits Construction Group Co., Ltd., Fuzhou 350014, China; clzheng896@csu.edu.cn

* Correspondence: zyzhou@csu.edu.cn



Citation: Liu, Q.; Xiao, J.; Cai, B.; Guo, X.; Wang, H.; Chen, J.; Zhang, M.; Qiu, H.; Zheng, C.; Zhou, Y. Numerical Simulation on the Effect of Fire Shutter Descending Height on Smoke Extraction Efficiency in a Large Atrium. *Fire* **2022**, *5*, 101. <https://doi.org/10.3390/fire5040101>

Academic Editors: Chuangang Fan and Dahai Qi

Received: 14 June 2022

Accepted: 15 July 2022

Published: 17 July 2022

Publisher's Note: MDPI stays neutral with regard to jurisdictional claims in published maps and institutional affiliations.



Copyright: © 2022 by the authors. Licensee MDPI, Basel, Switzerland. This article is an open access article distributed under the terms and conditions of the Creative Commons Attribution (CC BY) license (<https://creativecommons.org/licenses/by/4.0/>).

Abstract: In this study, a series of numerical simulations were carried out to investigate the effect of fire shutter descending height on the smoke extraction efficiency in a large space atrium. Based on the full-scale fire experiments, this paper carried out more numerical simulations to explore factors affecting the smoke extraction efficiency in the atrium. The smoke flow characteristics, temperature distribution law and smoke extraction efficiency of natural and mechanical smoke exhaust systems were discussed under different heat release rates and fire shutter descending heights. The results show that the smoke spread rate and the average temperature of the smoke are higher with a greater heat release rate. After the mechanical smoke exhaust system is activated, the smoke layer thickness and smoke temperature decrease, and the stable period of heat release rate is shorter. In the condition of natural smoke exhaust, the smoke extraction efficiency increases exponentially with the increase of heat release rate and the descending height of the fire shutter, and the maximum smoke extraction efficiency is 48.8%. In the condition of mechanical smoke exhaust, the smoke extraction efficiency increases with the increase of mechanical exhaust velocity. When the velocity increases to the critical value (8 m/s), the smoke extraction efficiency is essentially stable. The smoke extraction efficiency is increased first with the increase of fire shutter descending height and then has a downward trend when the descending height drops to half, and the maximum smoke extraction efficiency is 70.3% in the condition of mechanical smoke exhaust. Empirical correlations between the smoke extraction efficiency and the dimensionless fire shutter descending height, the dimensionless heat release rate and the dimensionless smoke exhaust velocity have been established. The results of this study can provide a reference for the design of smoke prevention and exhaust systems in the atrium.

Keywords: atrium fire; smoke extraction efficiency; fire shutter descending height; numerical simulation

1. Introduction

In recent years, an increasing number of urban commercial complexes have emerged, not only bringing great convenience to people's lives, but also causing greater fire hazards. The mall atrium is a large space which integrates shopping, entertainment, leisure and other functions. Usually, there are dense personnel and numerous combustibles in the mall atrium, which brings a high fire risk. Once a fire occurs, it is likely to spread to the buildings next to the atrium, which causes serious economic losses and casualties; moreover, smoke is the most critical factor that threatens the safety of people in fires. Therefore, it is of great significance to study the law of smoke spreading and smoke extraction efficiency

in the atrium and indoor pedestrian street, which is the key passage for personnel safety evacuation [1–3].

The research on the spread and control of fire smoke in large-space buildings started in the 1970s. Many scholars have studied the factors affecting the fire plume and smoke spread characteristics, and given many mathematical relationships through experiments, such as Thomas et al. [4], McCaffery [5,6], Zukoski et al. [7,8], Heskestad [9,10] and Tanaka et al. [11]. In addition, they established some theoretical models of axisymmetric fire plumes, which laid the theoretical foundation for the study of fire smoke development in large spaces. Since then, their results have been widely used in the prediction and control of fire smoke. With the increase of research by domestic and foreign scholars, the understanding of the fire smoke spread characteristics has gradually increased and a relatively complete system has been formed. In the 1990s, with the development of computational technology, the advantages of numerical simulation technology have gradually been highlighted, which has good visualization effects and simple operation methods. Nowadays, it has become the mainstream method of studying indoor large-space fire [12–16].

Fires generate a great deal of heat and smoke, which threaten people's lives. On the one hand, fire and smoke separations are required to hinder the further spread of fire and smoke; on the other hand, heat and smoke also need to be exhausted from the atrium by smoke vents. Therefore, the efficiency of smoke extraction is closely linked to the safe evacuation of people. Different smoke exhaust systems will cause different smoke flowing and temperature distribution laws. As a rule, mechanical smoke exhaust systems are more responsive and reliable than natural smoke exhaust systems, which are now widely used for fire and smoke extraction in large spaces. Many scholars have carried out exhaustive research on large space atrium fires. For example, Klote et al. [17,18] found the law and calculation method of smoke flow in atrium fire. Hadjisophocleous et al. [19–22] combined experiments and numerical simulation to analyze the smoke spread and filling characteristics of atrium fires, the calculation method of smoke layer height and the smoke extraction efficiency of the mechanical smoke exhaust system in the atrium. Rho and Ryou [23] studied the characteristics of smoke flow in a large space atrium by numerical simulation. Chow et al. [24–26] investigated the fire development form and the smoke flow characteristics of the atrium through numerical simulation and small-scale experiments. Wong [27] figured out the influence of the distance between the fire shutter and the evacuation distance of the emergency exit under various circumstances. Yu and Wei [28] ensured the safe distance from combustibles to the fire shutters in the atrium. Yu [29] aimed at the safety and reliability of the fire shutter.

Long et al. [30] carried out full-scale fire experiments for several vital parameters including the vertical temperature distribution, the longitudinal temperature distribution, smoke layer height and smoke front arrival time under four different scenarios. Huang et al. [31] found the enlargement of the difference between the two heights, and the smoke spread process became slower at the constant heat release rate. Zhang et al. [32] solved the impact of the segmented smoke exhaust of the ultra-thin and tall atrium on fire prevention and control by using a full-scale hot smoke experiment method. Xu's results via the fire dynamics simulator (FDS) indicate that the temperature is changed more sharply than the visibility while the ceiling height gets higher [16].

Although scholars have studied the smoke extraction efficiency of the atrium through experiments or simulations, there is little involved in the impact of the fire shutter on it. The existence of a fire shutter has significantly changed the fire situation; this results in a research gap.

A fire shutter is a facility used for fire protection, heat insulation and smoke prevention for buildings; it also has an effect on the efficiency of smoke extraction in large spaces. The descending height of the fire shutter will affect the airflow, thus affecting the smoke extraction efficiency; besides, the smoke extraction method (including natural smoke extraction and mechanical smoke extraction) also has an effect on the smoke extraction efficiency; however, current studies have not given the influence mechanism of fire shutter

on the smoke extraction effect. Therefore, this study is expected to reveal the relationship between the two parameters by numerical simulations.

2. Numerical Simulation Conditions

2.1. Governing Equations

The flow of smoke in a building fire exists in the form of turbulent flow. Several conservation laws should be followed in the process of turbulent flow, including conservation of mass, conservation of momentum, conservation of energy and conservation of components. Therefore, a turbulence model should be established when studying building fire, and so should the computer simulations. Various conservation laws are expressed in the form of governing equations, which are introduced below [33].

(1) Equations for conservation of mass

$$\frac{\partial \rho}{\partial t} + \frac{\partial(\rho u)}{\partial x} + \frac{\partial(\rho v)}{\partial y} + \frac{\partial(\rho w)}{\partial z} = 0 \tag{1}$$

where ρ is the air density, kg/m³; t is time, s; u, v, w are the vectors in direction x, y, z .

(2) Equations for conservation of momentum

$$\frac{\partial(\rho u)}{\partial t} + \frac{\partial(\rho uu)}{\partial x} + \frac{\partial(\rho uv)}{\partial y} + \frac{\partial(\rho uw)}{\partial z} = \frac{\partial}{\partial x} \left(\mu \frac{\partial u}{\partial x} \right) + \frac{\partial}{\partial y} \left(\mu \frac{\partial u}{\partial y} \right) + \frac{\partial}{\partial z} \left(\mu \frac{\partial u}{\partial z} \right) - \frac{\partial p}{\partial x} + S_u \tag{2}$$

$$\frac{\partial(\rho v)}{\partial t} + \frac{\partial(\rho vu)}{\partial x} + \frac{\partial(\rho vv)}{\partial y} + \frac{\partial(\rho vw)}{\partial z} = \frac{\partial}{\partial x} \left(\mu \frac{\partial v}{\partial x} \right) + \frac{\partial}{\partial y} \left(\mu \frac{\partial v}{\partial y} \right) + \frac{\partial}{\partial z} \left(\mu \frac{\partial v}{\partial z} \right) - \frac{\partial p}{\partial y} + S_v \tag{3}$$

$$\frac{\partial(\rho w)}{\partial t} + \frac{\partial(\rho wu)}{\partial x} + \frac{\partial(\rho wv)}{\partial y} + \frac{\partial(\rho ww)}{\partial z} = \frac{\partial}{\partial x} \left(\mu \frac{\partial w}{\partial x} \right) + \frac{\partial}{\partial y} \left(\mu \frac{\partial w}{\partial y} \right) + \frac{\partial}{\partial z} \left(\mu \frac{\partial w}{\partial z} \right) - \frac{\partial p}{\partial z} + S_w \tag{4}$$

where ρ is the air density, kg/m³; t is time, s; u, v, w are the vectors in direction x, y, z ; p is the pressure of fluid microelement, Pa; S_u, S_v, S_w are generalized source term.

(3) Equations for conservation of energy

$$\frac{\partial(\rho T)}{\partial t} + \frac{\partial(\rho u T)}{\partial x} + \frac{\partial(\rho v T)}{\partial y} + \frac{\partial(\rho w T)}{\partial z} = \frac{\partial}{\partial x} \left(\frac{k}{c_p} \frac{\partial T}{\partial x} \right) + \frac{\partial}{\partial y} \left(\frac{k}{c_p} \frac{\partial T}{\partial y} \right) + \frac{\partial}{\partial z} \left(\frac{k}{c_p} \frac{\partial T}{\partial z} \right) + S_T \tag{5}$$

where T is temperature, K; k is heat transfer coefficient; c_p is specific heat capacity, kJ/(kg·K); S_T is viscous dissipation term.

(4) Equations for conservation of component

$$\frac{\partial(\rho c_s u)}{\partial x} + \frac{\partial(\rho c_s v)}{\partial y} + \frac{\partial(\rho c_s w)}{\partial z} = \frac{\partial}{\partial x} \left(D_s \frac{\partial \rho c_s}{\partial x} \right) + \frac{\partial}{\partial y} \left(D_s \frac{\partial \rho c_s}{\partial y} \right) + \frac{\partial}{\partial z} \left(D_s \frac{\partial \rho c_s}{\partial z} \right) + S_s \tag{6}$$

where c_s is the volume concentration of component S ; D_s is the mass of the component S generated by the chemical reaction of unit time and unit volume

(5) Boundary condition

$$-k_s \frac{\partial T_s}{\partial t} = \dot{q}_c'' + \dot{q}_r'' \tag{7}$$

where q_c'' is convective heat transfer, W; q_r'' is radiant heat, W.

2.2. Physical Model

This study takes the indoor pedestrian street of a children’s hospital in Fujian Province as the model, which has 4 floors and the height is 4.5 m per floor. The pedestrian street is 154 m long and 17 m wide. The width of the ring corridor is 4 m and the height under

the ceiling is 2.8 m. The pedestrian street has three atriums, #1, #2 and #3, and the height of each atrium is 19.8 m (including the height of smoke storage bins). The #2 atrium is selected as the study object, which is 32.4 m long and 8 m wide. The fire shutters separate the ring corridor from the atrium, which is 7.3 m wide, 31.8 m long and 2.8 m high. During the experiments, the doors and windows on both sides of the ring corridor are closed. The volume of the smoke exhaust fan in this study is 64,200 m³/h as the actual experiment building is. The schematic diagram of the numerical model of the building complex is shown in Figure 1.

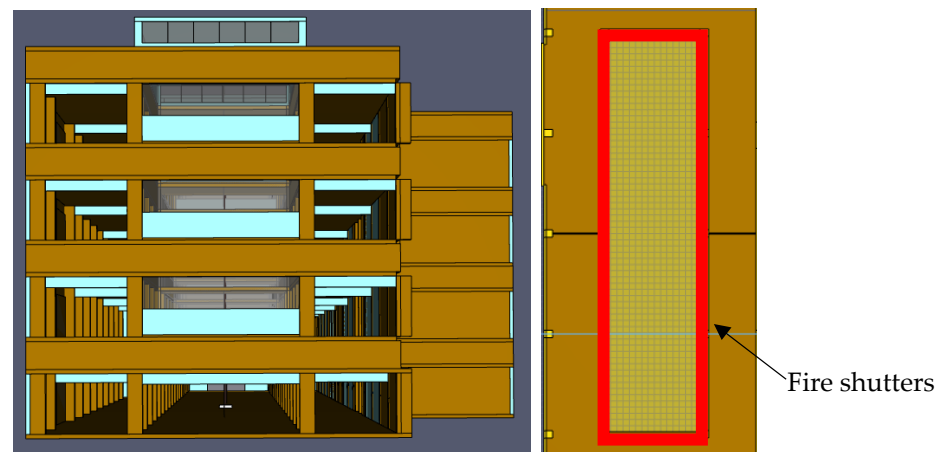


Figure 1. Schematic diagram of the numerical model of the building complex.

Fire usually occurs in the central location of the atrium floor, so the fire is set in the central location of the #2 atrium floor in this study. To simplify the calculation, the ground and structures are assumed to be adiabatic and the ambient temperature is 20 °C. The exterior walls are set as thermal insulation. There is no natural wind speed in the atrium. The atmospheric pressure is 101,325 Pa. In this study, ethanol is used as fuel to simulate the fire source with a t^2 fire model, which is assumed that the heat release rates keep constant after reaching the maximum. Besides, the temperature distribution and smoke extraction efficiency in the atrium are studied by numerical simulation under different fire shutter descending heights and exhaust conditions.

The fire shutter, the surface of which is made up of steel or inorganic fibre material, is a kind of fire prevention and heat insulation facility suitable for large openings in buildings. The fire shutters are driven through the transmission device and control system, playing a part of fire prevention and fire isolation; it is an indispensable fire prevention facility in modern buildings.

Heat release rate, smoke exhaust velocity, fire shutter descending height and exhaust method are selected as variables for numerical simulation. In total, 168 groups of experiments are designed. Three heat release rates are designed, 0.75 MW, 1.5 MW and 3.0 MW, respectively [34]. Eight smoke exhaust velocities are designed, ranging from 0 to 14 m/s with an interval of 2 m/s. The descending heights of the fire shutter are designed as 0 m, 0.7 m, 1.1 m, 1.4 m, 1.7 m, 2.1 m and 2.8 m, counting 7 groups.

Five thermocouples are arranged directly above the fire. The lowest thermocouple is 0.9 m away from the fire source, and the next is arranged every other 0.35 m upward, numbering 1–5 in sequence. The top thermocouple is 2.3 m away from the fire. More thermocouples are set from No. 5 thermocouples in the four directions, with an interval of 0.35 m, numbering 6–13 in turn. Thermocouples are arranged every other 1 m at the place 2.3 m away from the fire, and the highest one is 17.3 m, numbering V1–V16 from the top to the bottom. At the height of 9.3 m, 13.8 m and 18.3 m, 7 thermocouples are arranged along the centerline from west to east separately, with a horizontal distance interval of 1 m, numbering Z3F1–Z3F7, Z4F1–Z4F7, ZTH1–ZTH7. Temperature slices and visibility slices

are set at the central line of ring corridors in every floor and the atrium centre. Several gas detectors are set near the window at the rooftop to monitor CO₂ concentration.

2.3. Grid-Dependency Evidence

In FDS numerical simulation, the grid distribution of the computational region must correctly describe the variation of physical quantities in the flow field, as well as meet the computer workload. Therefore, a sensitivity analysis of the grid is required. In the meshing of the model, the mesh edge length is decremented from 0.6 m to 0.3 m with an interval of 0.1 m each time, and every condition is run separately. The temperature variation of each working condition is compared with the experimental value of the same point, and the calculation accuracy increases gradually with the decrease of grid edge length. When the temperature of the measurement point is very close to the experimental value, the grid size at this time is the ideal simulation grid size. Figure 2 shows the temperature variation of the same measurement point with the grid side length from 0.6 m to 0.3 m with an interval of 0.1 m; it is easy to find that when the grid size is 0.3 m, the temperature is very close to the experimental value. If the grid size is further decreased, it will not help much to improve the accuracy, but the computation volume will increase four times. Therefore, the size of the grid for numerical simulation is determined to be 0.3 m × 0.3 m × 0.3 m in this study under the premise of ensuring both computational accuracy and computational efficiency. As is shown in Figure 2, the numerical simulation results are in good agreement with the experimental results and the data error is within an acceptable range [35]. Therefore, we believe that the calculated results of the numerical simulation in this study are reliable.

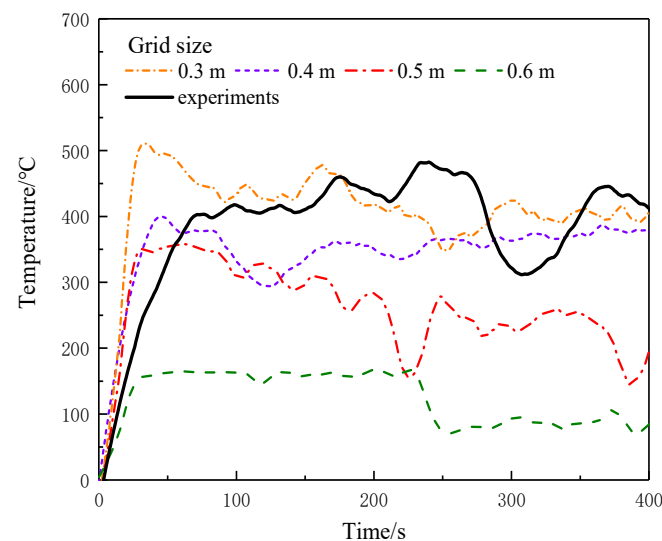


Figure 2. Temperature comparison chart for different grid sizes.

3. Results and Discussion

3.1. Smoke Spread Process

When a fire occurs, a large amount of smoke and heat will be generated to form a hot smoke flow, and the direction of smoke flow is often the direction of fire spread [36]. The smoke generated by the atrium fire will gradually converge over the atrium, and the smoke layer will continue to settle. Therefore, the visibility is constantly reduced and the visual range of evacuees is affected, slowing down the evacuation speed.

According to the principle of fire dynamics, fire development goes through three stages: accelerated combustion, stable combustion and extinction. Figure 3 shows the diagram of the smoke spread of fire inside the atrium at 30 s, 100 s and 300 s of the fire. Under the effect of thermal buoyancy, fire smoke rises first and spreads horizontally after reaching the ceiling. When the heat release rate is 0.75 MW, only a small amount of smoke is produced, and the height of smoke reaches half of the height of the atrium; after that, it

begins to generate more smoke. At 100 s, the smoke reaches the ceiling and spreads into the ring corridor. At 300 s, the smoke has filled the upper space of the atrium. When the heat release rate reaches 1.5 MW, smoke is generated more obviously and quickly. The atrium above the fourth floor is almost filled with smoke at 100 s. When the heat release rate comes to 3.0 MW, smoke only takes 30 s to reach the ceiling, then it begins to spread outside through the window of the top floor at 100 s. Due to the restriction of the walls of the atrium, the continuously generated smoke begins to settle, and there is a clear boundary between the smoke layer and the cold air layer.

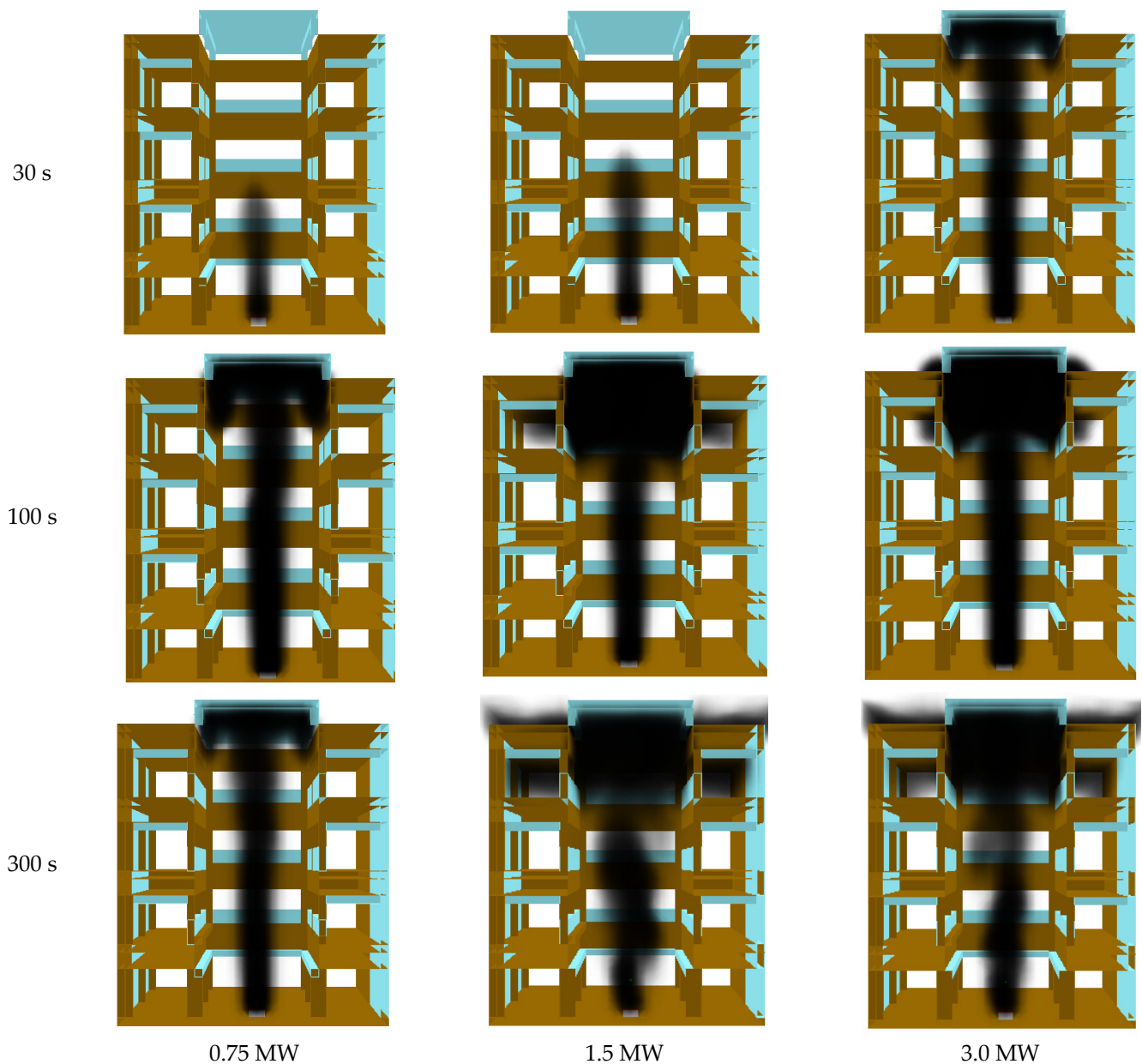


Figure 3. Diagram of the smoke spread of fire inside the atrium at different heat release rates and times.

There are significant differences in the rate of smoke spread under different heat release rates. In the case of a greater heat release rate, the smoke spread rate is faster, and the thickness of the stable smoke layer is significantly thicker. Obviously, the bigger the heat release rate is, the more obvious the heat buoyancy effect is, and the stronger the roll absorption effect is. Therefore, the smoke reaches the roof, gathers, and begins to settle

earlier with a bigger heat release rate. When the natural smoke and mechanical smoke exhausts are turned on, a significant reduction in the concentration and thickness of the smoke layer is shown. Because the opening smoke vent draws the smoke outside, reducing the concentration and the thickness of the smoke layer.

As a separation between the atrium and the ring corridor, the fire shutter hinders the smoke from spreading to the ring corridor to some extent. The descending height of the fire shutter has a certain influence on the time and rate of smoke spreading into the ring corridor. When the fire shutter is not activated (descending height is 0 m), the smoke can freely enter the ring corridor.

Visibility is the furthest distance that one can see the target object in a given environment; it is greatly reduced due to massive suspended particles and harmful gases in the smoke, hindering the safe evacuation of people. The minimum visibility in a large space is 10 m in fire [37]. Figure 4 shows the diagram of the visibility inside the atrium at 30 s, 100 s and 300 s. Visibility tends to decrease from the fire source to the top of the atrium. At 30 s, the rate and volume of smoke generation is small, so only vertical orientation at the central axis is affected. Visibility near the fire decreased to less than 15 m. Gradually, the smoke trends to enter the atrium and ring corridor. Relatedly, visibility in the ring corridor begins to decrease. Because most of the smoke is concentrated in the upper layer of the atrium, the visibility of the fourth layer is greatly affected, decreasing to 12 m at 100 s. Smoke fills the ring corridor when the fire develops stable at 300 s; at this time, visibility of the fourth ring corridor decreases to about 6 m, and the lower floors are less affected. Since the smoke does not spread to the lower floors, the visibility keeps in a normal range.

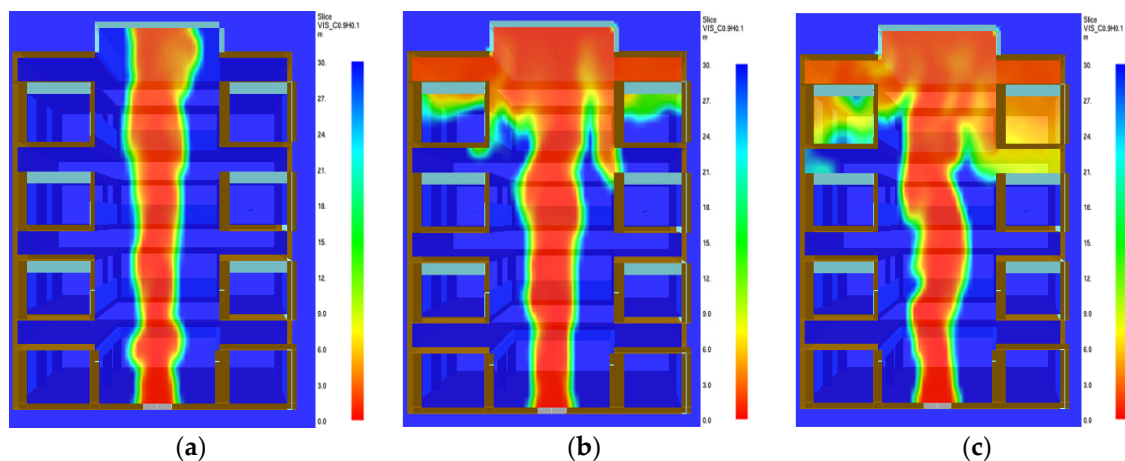


Figure 4. Diagram of the visibility inside the atrium at 30 s, 100 s and 300 s of the fire. (a) 30 s (b) 100 s (c) 300 s.

3.2. Temperature Distribution Law

A large amount of smoke and tremendous heat will be generated when a fire occurs. The hot environment and toxic smoke generated by the fire will make it difficult to evacuate the trapped people. Prolonged exposure to smoke can seriously damage a person's bodily functions and ability to escape.

Figure 5 shows the smoke temperature distribution inside the atrium at 30 s, 100 s and 300 s. At the early stage of the fire, less heat is released, so the smoke temperature rises relatively slowly. In the fire growth stage, the temperature gradient increases rapidly and reaches the maximum temperature quickly. With the decrease in heat release rate, the stable temperature value of the same measurement point nearest to the fire source decreases successively; it indicates that the greater the heat release rate is, the greater the average temperature of the smoke in the atrium is. The thermocouple closest to the fire source has the highest temperature, while the thermocouple farthest away has the lowest temperature. Because the smoke gradually loses heat as it moves farther up in the atrium. The maximum

temperature at the centre of the fire source can reach about 750 °C. The natural smoke exhaust mainly affects the smoke temperature in the upper part of the atrium, and has less influence on the smoke temperature close to the fire source; this is mainly because only the top window of the atrium is opened during natural smoke exhaust, which accelerates the flow of smoke near it and accelerates the heat exchange; however, it has little effect on the near-fire source location, which is farther away from the glass window.

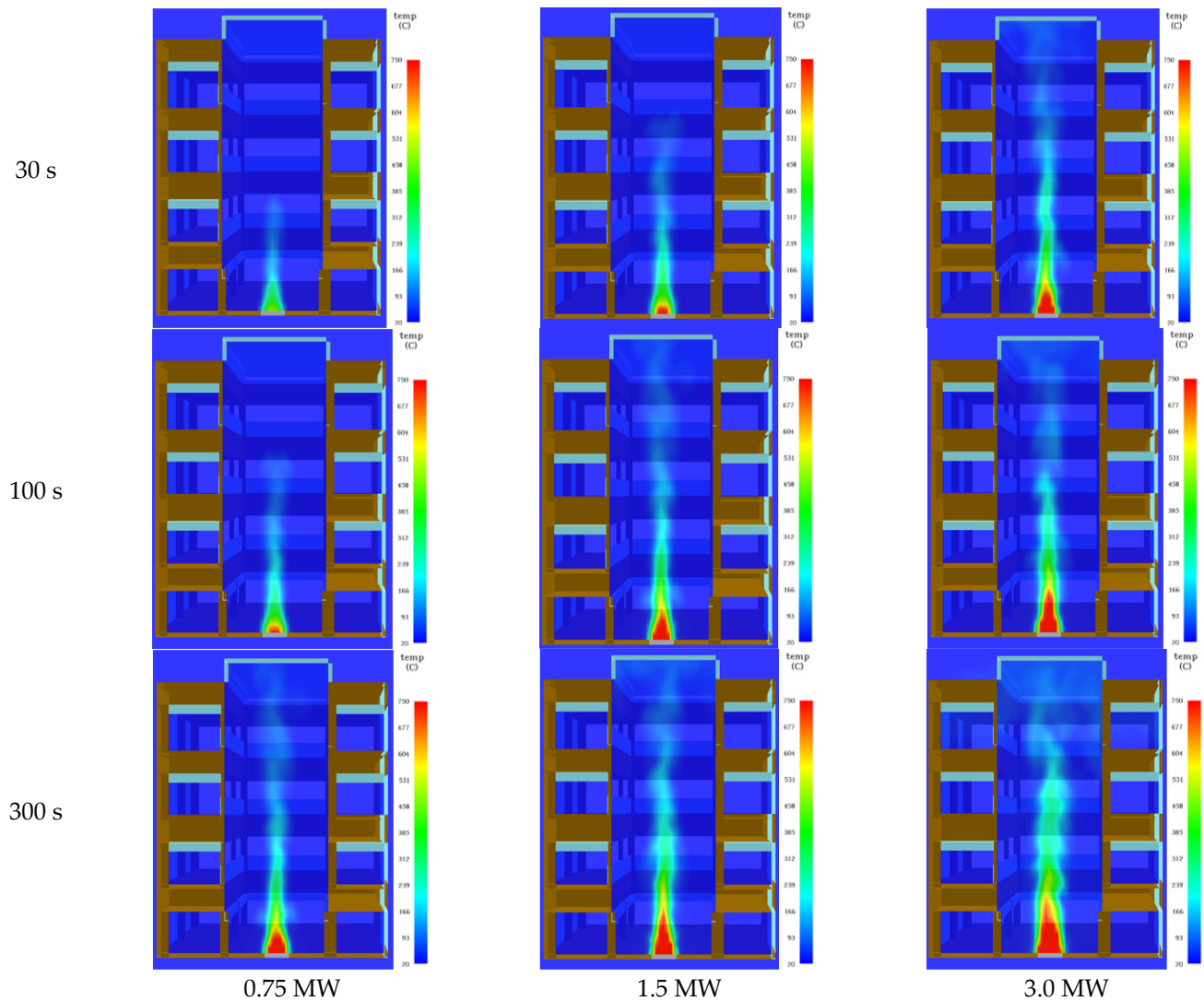


Figure 5. Fire smoke temperature distribution inside the atrium at different heat release rates and times.

3.3. Smoke Extraction Efficiency Analysis

The smoke extraction efficiency is defined as the percentage of smoke exhaust volume per unit time in the total amount of smoke generated, namely: smoke extraction efficiency = (smoke exhaust volume per unit time/the total amount of smoke generated per unit time) \times 100% [38]; however, it is difficult to measure the amount of smoke produced and discharged because of the various components of smoke and the different entrainment amount of surrounding air by the plume under the influence of different external conditions. Therefore, CO₂, the main combustion product of ethanol, is selected as the calculation index in the numerical simulation. The ratio of CO₂ emission volume per unit time to CO₂

production volume per unit time is used to characterize the smoke extraction efficiency of the smoke extraction system. Smoke extraction efficiency δ can be described as:

$$\delta = \frac{\text{CO}_2 \text{ emission volume per unit time}}{\text{CO}_2 \text{ production volume per unit time}} \quad (8)$$

The chemical reaction equation for ethanol combustion in FDS is as follows [33]:



The heat of combustion of ethanol $\Delta H = 27,000$ kJ/kg. Therefore, it can be concluded that: CO_2 production volume per unit time is 0.055 kg/s in 0.75 MW fire, 0.11 kg/s in 1.5 MW fire, 0.22 kg/s in 3.0 MW fire.

In this paper, considering smoke extraction efficiency δ is related to the heat release rate \dot{Q} and fire shutter descending heights h . A dimensionless analysis method is used to analyze the data.

Designing $\dot{Q}^* = \frac{\dot{Q}}{\rho_\infty c_p T_\infty \sqrt{g} H^{5/2}}$, $h^* = \frac{h}{H'}$, $v^* = \frac{v}{v_{crit}}$ [39], where \dot{Q} is total heat release rate; h is the descending height of the fire shutter; H' is the floor height; v is the smoke exhaust velocity; v_{crit} is the critical smoke exhaust velocity; ρ_∞ is the density of air around, 1.29 kg/m³; c_p is the specific heat capacity of air at constant pressure, 1.005 kJ/(kg·K); T_∞ is the ambient temperature, 293 K; g is the acceleration of gravity, 9.8 N/kg. We can find $\delta \sim f(\dot{Q}^*, h^*, v^*)$.

In the natural smoke exhaust mode, the relationship between the dimensionless descending height of the fire shutter and the smoke extraction efficiency is shown in Figure 6:

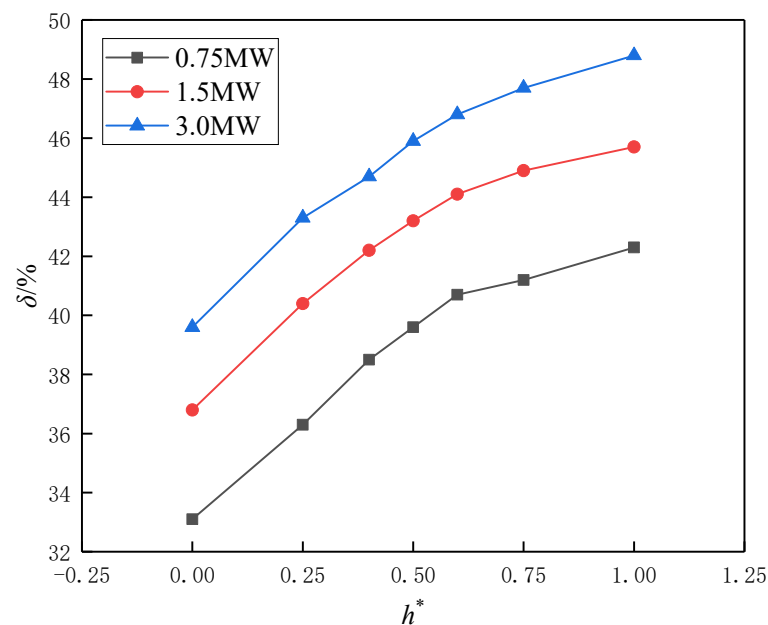


Figure 6. Relationship between the dimensionless descending height of the fire shutter and the smoke extraction efficiency.

In Figure 6, the smoke extraction efficiency increases steadily with the increase of fire shutter descending height in all conditions. In addition, the greater heat release rate possesses bigger smoke extraction efficiency, ranging from 39.6% to 48.8% at the biggest heat release rate while from 33.1% to 42.3% at the smallest heat release rate. When the heat release rate is 0.75 MW, the smoke extraction efficiency is only 33.1% if the fire shutter does not drop. The smoke extraction efficiency begins to increase along with the descending

of the fire shutter, finally up to 42.3%. The initial growth is slightly faster than the latter. Trends of the smoke extraction efficiency when the heat release rates are 1.5 MW and 3.0 MW are similar to that of 0.75 MW, respectively, from 36.8% to 45.7% and from 39.6% to 48.8%. The increase of heat release rate enhances the average temperature of the smoke in the large space; this weakens the effect of air mixing into the smoke to some extent, so that the smoke extraction efficiency increases, and this phenomenon becomes more obvious when the heat release rate is greater.

As is shown above, $\dot{Q}^* = \frac{\dot{Q}}{\rho_{\infty} c_p T_{\infty} \sqrt{g} H^{5/2}}$, $h^* = \frac{h}{H}$ we can easily find that \dot{Q}^* and h^* are independent of each other. Considering δ is a function about \dot{Q}^* and h^* , we assume that $\delta \sim (\dot{Q}^*)^m (h^*)^n$. Fitting the δ with \dot{Q}^* and h^* , respectively, we can get $\delta \sim (\dot{Q}^*)^{0.15}$, $\delta \sim (h^*)^{0.1}$. The relationship between δ and $(\dot{Q}^*)^{0.15} (h^*)^{0.1}$ is shown in Figure 7.

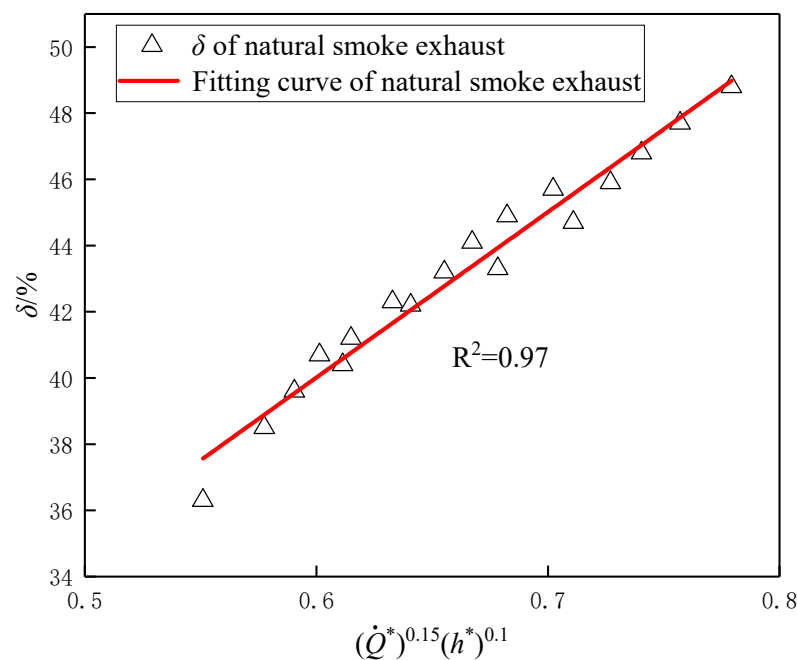


Figure 7. Natural smoke exhaust fitting line.

After linear fitting the data points above, we can find all the points fall almost near the same fit line. This line can be expressed as:

$$\delta = 10 + 50(\dot{Q}^*)^{0.15} (h^*)^{0.1} \tag{10}$$

Figure 7 shows a relationship between atrium smoke extraction efficiency and the dimensionless descending height of fire shutters and the dimensionless heat release rate. The points of abscissa are evenly distributed between 0.5 and 0.8. The natural smoke efficiency increases gradually from 36% to 48%. All the test points almost fall around the same line. The fitting coefficient R^2 reaches 0.97, which indicates a good fitting. Equation (10) can be empirically used to calculate the natural smoke extraction efficiency of the indoor pedestrian street atrium under the influence of a fire shutter.

Figure 8 shows the variation of smoke extraction efficiency δ with smoke exhaust velocity and descending height of fire shutters, under different heat release rates.

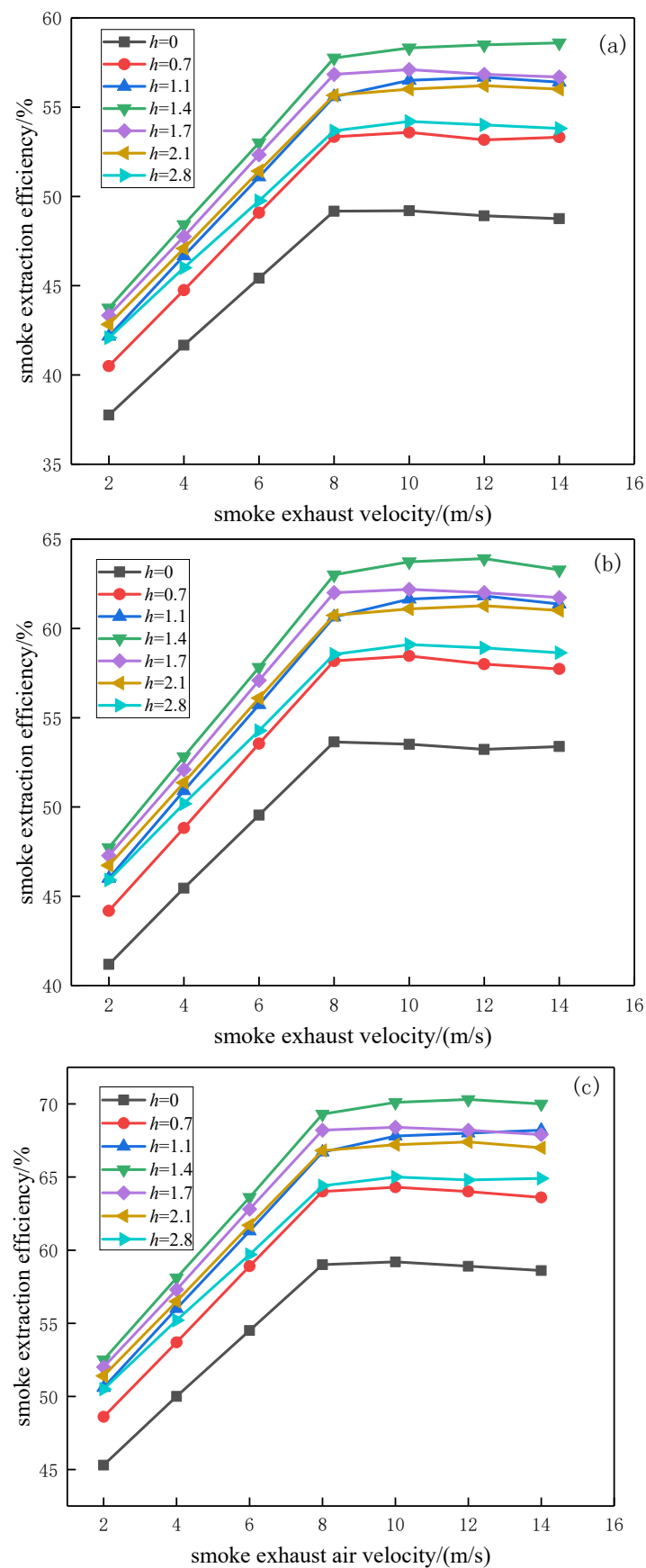


Figure 8. Curves of smoke extraction efficiency with smoke exhaust velocity and descending height of fire shutters at 0.75 MW, 1.5 MW, and 3.0 MW. (a) 0.75 MW (b) 1.5 MW (c) 3.0 MW.

When the smoke exhaust system is turned on, the air entrainment is intensified and the smoke rises with the air, so that the smoke extraction efficiency is gradually improved. When the fire shutter drops to a critical height of about 1.4 m (half of the floor height), the effect of the descending height on the smoke extraction efficiency is small, because the small space at the bottom restricts the air entrainment. As we can see, under different heat release rates, the smoke extraction efficiency at the critical height is stable at 58%, 64%, and 70%, respectively, with an interval of 6%.

In comparison, the efficiency of mechanical smoke exhaust is significantly higher than that of natural smoke exhaust. Because the smoke is continuously discharged from the atrium by the exhaust fan, which led to a better smoke extraction effect; thus, we suggest the atrium of the mall adopts the mode of combining natural smoke exhaust and mechanical smoke exhaust. Ordinarily, the natural smoke exhaust windows take the function of natural ventilation and smoke exhaust. Once a fire occurs, the mechanical smoke exhaust turns on and the fire shutters fall immediately. When the smoke exhaust air velocity stabilizes at 8 m/s and the fire shutters drop to half the floor height, the smoke extraction efficiency can reach the maximum.

It can be seen from Figure 8 that the smoke extraction efficiency in the mechanical smoke exhaust mode shows a trend of increasing at first with the increase of smoke exhaust velocity and then stabilizing after reaching a critical number. When the smoke exhaust velocity increases to 8 m/s, the mechanical smoke extraction efficiency is basically unchanged, regardless of the heat release rate. Therefore, we only analyze the increase stage of smoke extraction efficiency and ignore the stability stage. The dimensionless heat release rate \dot{Q}^* has no direct connection with dimensionless descending height h^* and dimensionless smoke exhaust velocity v^* . Therefore, it can be understood that \dot{Q}^* is independent with h^* and v^* . For the heat release rate of 3.0 MW, the variation law of δ with h^* and v^* are shown in Figures 9 and 10.

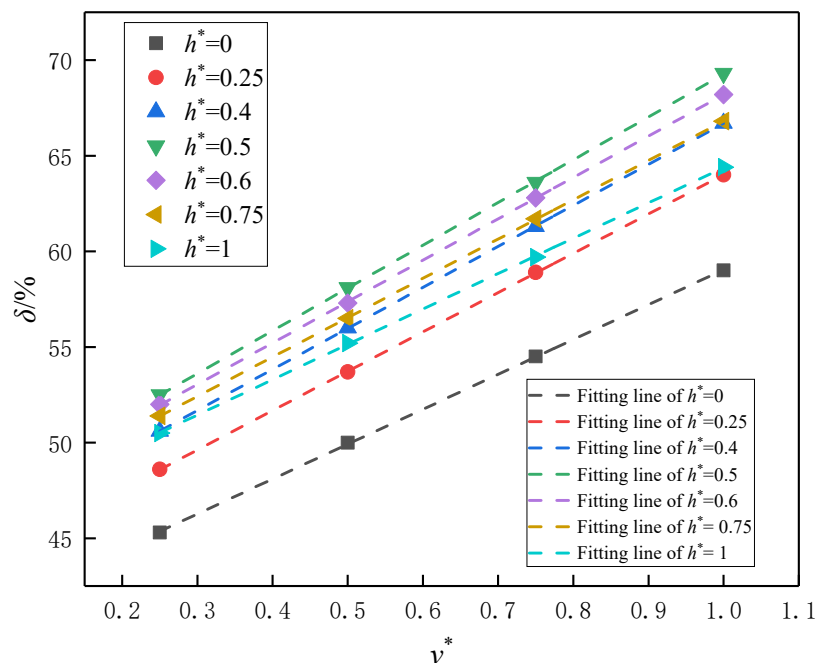


Figure 9. The relationship between δ and v^* when \dot{Q} is 3.0 MW.

It can be seen from Figure 9 that δ and v^* show a linear positive correlation. The fitted linear relationship is shown in Table 1.

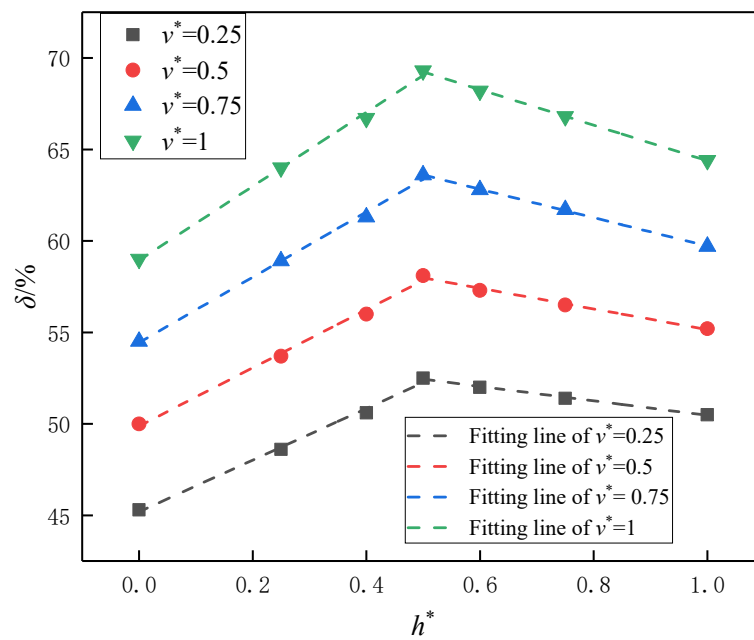


Figure 10. The relationship between δ and h^* when \dot{Q} is 3.0 MW.

Table 1. Results between δ and v^* .

Equation	$\delta = a + bv^*$						
h^*	0	0.25	0.4	0.5	0.6	0.75	1
Intercept	40.8	43.5	45.3	46.9	46.6	46.3	45.9
Slope	18.3	20.6	21.4	22.4	21.6	20.6	18.5
R ²	0.99	0.99	0.99	0.99	0.99	0.99	0.99

The slope has good symmetry about the centre position and is related to dimensionless descending height h^* . This means v^* shows a symmetric function about δ ; thus, the slope can be expressed as $8|2.8 - (0.5 - h^*)|$. In other words, $\delta \sim f(h^*) + 8|2.8 - (0.5 - h^*)|f(v^*)$.

It can be seen from Figure 9 that δ and v^* show a symmetrical linear positive correlation; however, δ first linearly increases and then linearly decreases with the increase of h^* . Therefore, we describe the relationship between them in two parts, as Tables 2 and 3 shows.

Table 2. Results between δ and v^* (when $h \leq 1.4$ m ($h^* \leq 0.5$)).

Equation	$\delta = a + bh^*$			
v^*	0.25	0.5	0.75	1
Intercept	45.2	49.9	54.4	58.9
Slope	14.2	15.9	17.9	20.2
R ²	0.99	0.99	0.99	0.99

Table 3. Results between δ and v^* (when $h \geq 1.4$ m ($h^* \geq 0.5$)).

Equation	$\delta = a + bh^*$			
v^*	0.25	0.5	0.75	1
Intercept	54.4	60.8	67.5	70.1
Slope	−3.9	−5.7	−7.8	−9.7
R ²	0.99	0.99	0.99	0.99

When $h \leq 1.4$ m ($h^* \leq 0.5$), v^* shows a positive correlation with δ . The relation expression can be $\delta \sim [45.2 + 14.2h^* + f(v^*)]$; when $h \geq 1.4$ m ($h^* \geq 0.5$), v^* shows a negative correlation with δ . The relation expression can be $\delta \sim [52.5 - 4.3(h^* - 0.5) + f(v^*)]$. Therefore, $f(h^*, v^*)$ can be expressed as:

$$f(h^*, v^*) = \begin{cases} 45.2 + 14.2h^* + 8(2.3 + h^*)(v^* - 0.25) & (h^* \leq 0.5) \\ 52.5 - 4.3(h^* - 0.5) + 8(3.3 - h^*)(v^* - 0.25) & (h^* \geq 0.5) \end{cases} \quad (11)$$

Furthermore, take the heat release rate \dot{Q}^* into account, the relationship turns $\delta \sim \dot{Q}^{*m} f(h^*, v^*)$. The relationship between δ and $\dot{Q}^{*m} f(h^*, v^*)$ at different descending heights is shown in Figure 11. The fitting results show that the theoretical formula matches the actual results and is reliable.

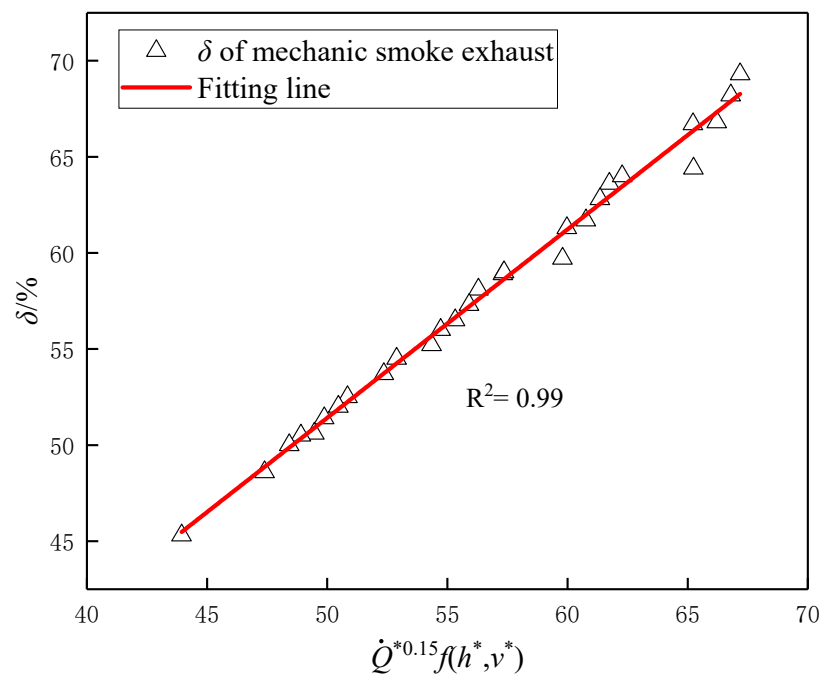


Figure 11. Relationship between δ and $\dot{Q}^{*0.15} f(h^*, v^*)$.

Therefore, when the mechanical smoke exhaust system is turned on, there is the following relationship between smoke extraction efficiency and smoke exhaust velocity and descending height of the fire shutter:

$$\delta = \dot{Q}^{*0.15} f(h^*, v^*) = \begin{cases} \dot{Q}^{*0.15} [45.2 + 14.2h^* + 8(2.3 + h^*)(v^* - 0.25)] & (h^* \leq 0.5) \\ \dot{Q}^{*0.15} [52.5 - 4.3(h^* - 0.5) + 8(3.3 - h^*)(v^* - 0.25)] & (h^* \geq 0.5) \end{cases} \quad (12)$$

4. Discussion and Conclusions

In this paper, the effect of the descending height of the fire shutter on the smoke spread law and smoke extraction efficiency in the atrium is studied by numerical simulation. When the fire heat release rate is small, the smoke subsidence speed in natural smoke exhaust mode is faster than that of mechanical smoke exhaust mode. At the same time, mechanical smoke exhaust can discharge a large amount of smoke and take away a large amount of heat in a timely manner. The mechanical smoke exhaust makes the temperature lower than that of natural smoke exhaust at the same time and measuring point.

In the large space of the shopping mall atrium, the natural smoke efficiency is lower than that of mechanical smoke exhaust. The efficiency of the natural smoke exhaust is about 40%, and the efficiency of the mechanical smoke exhaust is about 60%. Besides, some factors can also affect the smoke extraction efficiency of mechanical smoke exhaust,

such as the heat release rate, the descending height of the fire shutter, and the smoke exhaust velocity.

After directional analysis, we draw some important conclusions as follows:

(1) With the increase of heat release rate from 0.75 MW to 3.0 MW, the smoke is generated and spreads faster. Besides the heat release rate being higher, the thickness of the stable smoke layer is significantly thicker than that with a lower heat release rate.

(2) When the heat release rate is lower than 1.5 MW, the subsidence rate of smoke in natural exhaust mode is faster than that in mechanical exhaust mode. The mechanical smoke exhaust system can discharge a large amount of smoke and heat in time, and the temperature at the same location is lower than using the natural smoke exhaust mode at the same time.

(3) In the natural smoke exhaust mode, the smoke extraction efficiency increases with the heat release rate and the descending height of the fire shutter, up to 48.8%. Empirical formula expression is expressed as Equation (12). The smoke flow is accelerated and the smoke extraction efficiency is increased, when the mechanical smoke exhaust system is turned on. The smoke extraction efficiency improves by 12% with the increase of the smoke exhaust velocity from 0 to 14 m/s. There is an upper limit value when the velocity is about 8 m/s, after which the smoke extraction efficiency is stable. Smoke extraction efficiency first increases with the increase of descending height. When the fire shutter down to half, the smoke extraction efficiency shows a downward trend. Smoke extraction efficiency reaches up to 70.3% after turning on the mechanical smoke extraction system. The empirical equation of smoke extraction efficiency has been established and the mechanical smoke extraction efficiency is about 20% higher than that of natural smoke extraction efficiency.

Although this paper takes a children's hospital as a model for experimental research, the conclusions can still be applied to other related structures, especially buildings with a large atrium and fire shutters. Whereas fire shutter plays a more and more important role in modern intelligent architecture, there is a lack of relative research on the influence of fire shutter on the smoke extraction effect. The results of this study can possess a guiding significance for the smoke control design of the architecture.

Author Contributions: Conceptualization, Q.L. and Y.Z.; methodology, Y.Z.; software, Q.L. and J.X.; validation, J.X., B.C. and Y.Z.; formal analysis, Q.L.; investigation, X.G.; resources, H.W.; data curation, J.C. and Q.L.; writing—original draft preparation, Q.L.; writing—review and editing, Q.L. and Y.Z.; visualization, B.C., X.G. and M.Z.; supervision, H.Q. and C.Z.; project administration, C.Z.; funding acquisition, J.X. and X.G. All authors have read and agreed to the published version of the manuscript.

Funding: This work was supported by the Regional Development Science and Technology Program of Fujian Province (No. 2019Y3002) and Natural Science Foundation of Hunan Province (No. 2021JJ30860).

Conflicts of Interest: The authors declare no conflict of interest.

References

1. Zheng, W. Fire safety design of indoor pedestrian streets of large commercial building. *Procedia Eng.* **2013**, *52*, 652–656. [[CrossRef](#)]
2. Xu, X.; Wang, Z.; Liu, X.; Ji, C.; Yu, N.; Zhu, H.; Li, J.; Wang, P. Study on Fire Smoke Control in Super-high Building Atrium. *Procedia Eng.* **2018**, *211*, 844–852. [[CrossRef](#)]
3. Wang, R.; Lan, X.; Xu, L. Smoke spread process under different heights based on numerical simulation. *Case Stud. Therm. Eng.* **2020**, *21*, 100710. [[CrossRef](#)]
4. Thomas, P.H.; Webster, C.T.; Raftery, M.M. Some experiments on buoyant diffusion flames. *Combust. Flame* **1961**, *5*, 359–367. [[CrossRef](#)]
5. McCaffery, B.J. *Purely Buoyant Diffusion Flames: Some Experimental Results*; National Bureau of Standards: Washington, DC, USA, 1979.
6. McCaffery, B.J. Momentum implications for buoyant diffusion flames. *Combust. Flame* **1983**, *52*, 149–167. [[CrossRef](#)]
7. Zukoski, E.E. Development of a stratified ceiling layer in the early stage of closed room fire. *Fire Mater.* **1978**, *2*, 54–62. [[CrossRef](#)]
8. Zukoski, E.E.; Kubota, T.; Cetegen, B. Entrainment in fire plumes. *Fire Saf. J.* **1981**, *3*, 107–121. [[CrossRef](#)]
9. Heskestad, G. Virtual origins of fire plumes. *Fire Saf. J.* **1983**, *5*, 109–114. [[CrossRef](#)]

10. Heskestad, G. Engineering relations for fire plumes. *Fire Eng. J.* **1984**, *7*, 25–32. [[CrossRef](#)]
11. Tanaka, T.; Fujita, T.; Yamaguchi, J. Investigation into Rise Time of Buoyant Fire Plume Fronts. *Int. J. Eng. Perform. Based Fire Codes* **2000**, *2*, 14–25.
12. Gutiérrez-Montes, C.; Sanmiguel-Rojas, E.; Viedma, A.; Rein, G. Experimental data and numerical modelling of 1.3 and 2.3 MW fires in a 20 m cubic atrium. *Build. Environ.* **2009**, *44*, 1827–1839. [[CrossRef](#)]
13. Qin, T.; Guo, Y.; Chan, C.; Lin, W. Numerical simulation of the spread of smoke in an atrium under fire scenario. *Build. Environ.* **2009**, *44*, 56–65. [[CrossRef](#)]
14. Ray, S.; Gong, N.; Glicksman, L.R.; Paradiso, J. Experimental characterization of full-scale naturally ventilated atrium and validation of CFD simulations. *Energy Build.* **2014**, *69*, 285–291. [[CrossRef](#)]
15. Zhang, G.; Zhou, X.; Zhu, G.; Yan, S. A new accident analysis and investigation model for the complex building fire using numerical reconstruction. *Case Stud. Therm. Eng.* **2019**, *14*, 100426. [[CrossRef](#)]
16. Xu, L.; Wang, Y.; Song, L. Numerical research on the smoke spread process of thin-tall atrium space under various ceiling height. *Case Stud. Therm. Eng.* **2021**, *25*, 100996. [[CrossRef](#)]
17. Klote, J.H. Prediction of smoke movement in atria: Part I—Physical concepts. *ASHRAE Trans.* **1997**, *103*, 534–544.
18. Klote, J.H. Prediction of smoke movement in atria: Part II—Application to smoke management. *ASHRAE Trans.* **1997**, *103*, 545–553.
19. Hadjisophocleous, G.V.; Loughheed, G.D.; Cao, S. Numerical study of the effectiveness of atrium smoke exhaust systems. *ASHRAE Trans.* **1999**, *105*, 1–17.
20. Loughheed, G.D. Investigation of atrium smoke exhaust effectiveness. *ASHRAE Trans.* **1997**, *103*, 519–533.
21. Loughheed, G.D.; Hadjisophocleous, G.V.; Mecartney, C.; Taber, B.C. Largescale physical model studies for an atrium smoke exhaust system. *ASHRAE Trans.* **1999**, *105*, 676–698.
22. Rafinazari, A.; Hadjisophocleous, G.V. An investigation of the effect of make-up air velocity on smoke layer height with asymmetric openings and rotational air flow in atrium fires. *J. Build. Eng.* **2020**, *27*, 100933. [[CrossRef](#)]
23. Rho, J.S.; Ryou, H.S. A numerical study of atrium fires using deterministic models. *Fire Saf. J.* **1999**, *33*, 213–229. [[CrossRef](#)]
24. Chow, W.K. Smoke Movement and Design of Smoke Control In Atrium Building—Part2 Diagrams. *Int. J. Hous. Sci. Its Appl.* **1990**, *14*, 147–159.
25. Chow, W.K. Simulation of The Atrium Fire Environment in Hong Kong. *ASHRAE Trans.* **1993**, *99*, 163–168.
26. Chow, W.K. A Short Note on the Simulation of Atrium Smoke Filling Process Using Fire Zone Models. *J. Fire Sci.* **1994**, *12*, 516–528. [[CrossRef](#)]
27. Wong, L.T. Evaluation of Safe Distance of Fire rolling shutters in Shopping Malls. *Archit. Sci. Rev.* **2003**, *4*, 403–409. [[CrossRef](#)]
28. Yu, J.J.; Wei, G.Z. Distance from combustibles to fire rolling shutter of a large commercial building. *Fire Sci. Technol.* **2014**, *1*, 63–66.
29. Yu, H.C. The discussion of fire rolling shutter reliability. *Fire Sci. Technol.* **2014**, *6*, 701–703.
30. Long, Z.; Liu, C.; Yang, Y.; Qiu, P.; Tian, X.; Zhong, M. Full-scale experimental study on fire-induced smoke movement and control in an underground double-island subway station. *Tunn. Undergr. Space Technol.* **2020**, *103*, 103508. [[CrossRef](#)]
31. Huang, Y.; Wang, E.; Bie, Y. Simulation investigation on the smoke spread process in the large-space building with various height. *Case Stud. Therm. Eng.* **2020**, *18*, 100594. [[CrossRef](#)]
32. Zhang, H.; Wang, J.; Du, C. Experimental study on the effect of segmented smoke exhaust on smoke exhaust of ultra-thin and tall atrium. *Case Stud. Therm. Eng.* **2021**, *28*, 101560. [[CrossRef](#)]
33. Li, S.; Li, X. *FDS Fire Numerical Simulation*; Chemical Industry Press: Beijing, China, 2019.
34. GA/T 999-2012; Test Method for Verifying, Field Performance of Smoke Management System—Hot Smoke Test. The Ministry of Public Security of the People's Republic of China, Standards Press of China: Beijing, China, 2012.
35. Jiao, A.; Lin, W.; Cai, B.; Wang, H.; Chen, J.; Zhang, M.; Xiao, J.; Liu, Q.; Wang, F.; Fan, C. Full-scale experimental study on thermal smoke movement characteristics in an indoor pedestrian street. *Case Stud. Therm. Eng.* **2022**, *34*, 102029. [[CrossRef](#)]
36. Zhong, M.; Li, P.; Liu, T. Experimental study on fire smoke movement in a multi-floor and multi-room building. *Sci. China Ser. E Eng. Mater. Sci.* **2005**, *48*, 292–304. [[CrossRef](#)]
37. Hall, J.R. U.S. high-rise fires: The big picture. *NFPA J.* **1994**, *88*, 47–53.
38. Pan, Y.; Zhao, H.; Wu, D.; Li, W. Study on smoke exhaust efficiency under central exhaust mode in tunnel fires. *J. Saf. Environ.* **2012**, *12*, 191–196.
39. Hurley, M.J.; Gottuk, D.; Hall, J.R.; Harada, K.; Kuligowski, E.D.; Puchovsky, M.; Torero, J.L.; Watts, J.M.; Wiecek, C.J. *SFPE Handbook of Fire Protection Engineering*, 5th ed.; Hurley, M.J., Ed.; Springer: New York, NY, USA; Berlin/Heidelberg, Germany; Dordrecht, The Netherlands; London, UK, 2019.